



Luminescent Pyrene-based Schiff base Receptor for Hazardous Mercury(II) Detection Demonstrated by Cell Imaging and Test Strip

Chethanakumar¹ · Mahantesh Budri¹ · Kalagouda B. Gudasi¹ · Ramesh S. Vadavi¹ · Satish S. Bhat¹

Received: 22 September 2022 / Accepted: 1 November 2022 / Published online: 30 November 2022
© The Author(s), under exclusive licence to Springer Science+Business Media, LLC, part of Springer Nature 2022

Abstract

Qualitative and quantitative analysis of mercury at concentration levels as low as parts per billion (ppb) is a basic and practical concern. The vast majority of research in this field has centered on the development of potent chemosensor to monitor mercuric (Hg^{2+}) ions. Mercury exists in three oxidation states, +2, +1 and 0, all of which are highly poisonous. In this study, (*N*¹*E*,*N*²*E*)-*N*¹,*N*²-bis(pyrene-1-ylmethylene)benzene-1,2-diamine (PAPM), a novel photoluminescent sensor based on pyrene platform was synthesized. Over the tested metal ions (Cd^{2+} , Co^{2+} , Cu^{2+} , Mg^{2+} , Mn^{2+} , Ni^{2+} , K^+ , Na^+ , Zn^{2+} , Sr^{2+} , Pb^{2+} , Al^{3+} , Cr^{3+} and Fe^{3+}) the sensor responds only to Hg^{2+} by showing high selectivity and sensitivity. After treatment with mercuric ions at room temperature, the luminescence intensity of probe was quenched at 456 nm. The quenching of fluorescence intensity of probe upon addition of mercury is due to the effect of “turn-off” chelation enhanced quenching (CHEQ) by the formation of 1:1 complex. The ESI–MS spectrum and the Job’s experimental results confirm the formation of 1:1 complex between PAPM and Hg^{2+} . The detection limit and association constant of sensor for mercury is computed using fluorescence titration data and were found to be 9.0×10^{-8} M and 1.29×10^5 M⁻¹ respectively. The practical application of sensor towards recognition of mercury(II) ions was explored through economically viable test strips and also using cell imaging studies.

Keywords Selective · Mercury(II) · Fluorescence quenching · Detection limit · Cell imaging and test strips

Introduction

Studies relevant to the detection and quantification of heavy and transition-metal ions have been appealing due to their exceedingly hazardous impact on the environment and biological systems [1]. Among various toxic heavy metal ions, the mercury ion (Hg^{2+}) is one of the most poisonous and endangering both human health and the environment [2] because it is released into environment by natural processes and human activities like water erosion, solid waste incineration, wind erosion, forest fires, oceanic and volcanic eruptions, fossil fuel combustion and industrial productions [3, 4]. Despite its toxicity, mercury compounds find variety of applications in industrial processes and products, including paints, electrical materials and batteries [5]. The presence of

mercury even at very low concentrations can accumulate in the human body and produce many health issues, including foetal brain damage, significant cognitive and motor abnormalities and minamata sickness [6]. Furthermore, due to more soft nature of mercury ions, it has a strong binding affinity towards thiol groups in proteins, which causes cell dysfunction and numerous diseases including kidney disorder, abdominal pain and nausea. In addition, mercury has the power to create various hormonal imbalance and problems in thyroidal system by quickly entering through skin and respiratory cell membranes in living system [7–9]. Hence, the need for highly selective and sensitive determination of mercury(II) ions is vital.

In literature, many analytical methods were reported for recognition of mercury(II) ions including neutron activation analysis, plasmon-resonance rayleigh scattering spectroscopy (RSS), graphite furnace atomic absorption spectrometry (GF-AAS), anodic stripping voltammetry, cold vapor atomic absorption spectroscopy (CV-AAS), cold vapor atomic fluorescence spectrometry (CV-AFS), atomic absorption spectroscopy, inductively coupled plasma mass spectrometry and emission spectroscopy. Although these

✉ Kalagouda B. Gudasi
drkbudasi@kud.ac.in

✉ Ramesh S. Vadavi
rsvadavi@gmail.com

¹ Department of Chemistry, Karnatak University, Dharwad 580003, India

methods are well established, they are expensive, time-consuming and can require complex sample preparation [10–15]. Due to its low cost, simplicity, superior sensitivity, simple instrumentation, low detection limit, real-time response, and non-destructive nature, sensing by fluorescence technique is typically preferred over above discussed methods for quantifying Hg^{2+} [16–22].

Schiff base (-C=N-) based fluorophores have demonstrated excellent results among various chemosensors due to their ease of synthesis and ability to provide a suitable electronic/geometrical environment after complexation with metal ions. Generally Schiff base based sensors are designed using aromatic, poly-aromatic units or heterocyclic moieties with conjugated double bond systems. By incorporating fluorescence assisting groups in Schiff base structural framework fluorescence property can be achieved. In addition to this the nitrogen atom of -C=N- group is well known for binding mercury and resulting complex exhibits biological and photophysical application. Including several environmental and biological applications, the Schiff base based sensors and their complexes have demonstrated anticancer, antibacterial, analgesic, antifungal, anti-inflammatory, antiviral, antioxidant, anti-malarial, antiglycation, and anti-ulcerogenic properties [23–26].

Several chemosensors containing sulphur and nitrogen donor atoms have been exploited for sensing of mercury(II) ions. Many of these sensors were developed through difficult synthetic routes and demonstrated poor selectivity towards Hg^{2+} . The detection limit of these fluorophores for mercury(II) ions was found between 0.2 and 12.0 μM [27–30]. Additionally, the sulphur containing receptors cause cell malfunctions and subsequently leads to many diseases in the biological system [31, 32]. Thus, the designing and developing sensors with nitrogen binding sites for the selective recognition of soft mercury(II) ions might be an ideal choice. The simple synthesis of ratiometric fluorescent chemosensors typically involves pyrene units due to its peculiar signal of excimer-to-monomer emission. Due to its high chemical stability, unique photophysical properties and remarkable fluorescence detection, pyrene derivatives have been exploited regularly as a fluorescence probe [33–40].

For biological and environmental applications, there is still a need for highly selective and sensitive fluorescent sensor which can only respond to mercury(II) ions. Hence, it is crucial and highly prized to develop a very sensitive and selective fluorescent chemosensors for quantification of Hg^{2+} [41, 42].

Herein, we report synthesis and characterization of a novel sulphur free, highly selective and sensitive molecular sensor for mercury(II) ions detection based on pyrene

as a backbone with limit of detection 9.0×10^{-8} M and its bio-imaging studies along with test strips practical applications. The following Table 1 shows comparison of reported mercury(II) sensor with present work.

Experimental

Materials and Methods

The chemicals and reagents used in the experiments were all analytical or spectroscopic grade. The inorganic metal nitrate salts $\text{Mg}(\text{NO}_3)_2 \cdot 6\text{H}_2\text{O}$, $\text{Cd}(\text{NO}_3)_2 \cdot 4\text{H}_2\text{O}$, $\text{Hg}(\text{NO}_3)_2 \cdot \text{H}_2\text{O}$, $\text{Co}(\text{NO}_3)_2 \cdot 6\text{H}_2\text{O}$, $\text{Ni}(\text{NO}_3)_2 \cdot 6\text{H}_2\text{O}$, $\text{Cu}(\text{NO}_3)_2 \cdot 3\text{H}_2\text{O}$, $\text{Zn}(\text{NO}_3)_2 \cdot 6\text{H}_2\text{O}$, $\text{Pb}(\text{NO}_3)_2$, $\text{Mn}(\text{NO}_3)_2 \cdot 4\text{H}_2\text{O}$, NaNO_3 , KNO_3 , $\text{Sr}(\text{NO}_3)_2$, $\text{Al}(\text{NO}_3)_3 \cdot 9\text{H}_2\text{O}$, Anhydrous FeCl_3 , $\text{CrCl}_3 \cdot 6\text{H}_2\text{O}$, mercury(II) acetate, o-phenylene diamine (OPD) and 1-pyrene carboxaldehyde were purchased from Sigma Aldrich. The entire UV–Visible and fluorescence studies were done by taking Milli-Q water. The elemental analysis (C, H and N) was carried out using Thermoquest CHN analyzer. The IR spectra were obtained using a Nicolet 6700 FT-IR spectrometer. In DMSO-d_6 , $^1\text{H-NMR}$ spectra were collected using a Jeol 400 MHz FTNMR spectrometer. Mass spectra were recorded using a Waters-USA Xevo G2-XS Qtof mass spectrometer. A Jasco-P-670 UV–Visible spectrophotometer was used to collect electronic spectra in 200–800 nm range. The Hitachi F-7000 Fluorescence Spectrophotometer was used to measure the fluorescence spectra.

Synthesis of Sensor PAMP (Scheme 1)

To the methanolic solution of OPD (0.5 g, 4.62 mmol, in 10 mL), a solution of 1-pyrene carboxaldehyde (2.12 g, 9.25 mmol, in 20 mL MeOH) was added dropwise at room temperature with steady stirring. To this, acetic acid (0.5 mL) was added and reaction mixture was boiled under reflux for 16 h. The completion of the reaction was confirmed by TLC. The precipitated yellow compound was filtered, washed with methanol (25 mL) and dried in air. The product has been recrystallized from mixture of chloroform and methanol (1:1). Yield: 2.42 g, 98%. M.P. 225–227 °C. Elem. Anal. Calculated for $\text{C}_{40}\text{H}_{24}\text{N}_2$: C, 90.20; H, 4.54; N, 5.26. Found: C, 90.17; H, 4.48; N, 5.21. $^1\text{H-NMR}$ (400 MHz, DMSO-D_6) δ 9.48 (s, 2H), 8.52 (d, $J=8.0$ Hz, 2H), 8.44 (d, $J=8.1$ Hz, 2H), 8.36–8.23 (m, 11H), 8.11 (t, $J=8.0$ Hz, 3H), 7.81 (s, 2H), 7.24 (s, 2H). $^{13}\text{C-NMR}$ (101 MHz, DMSO-D_6) δ 152.27,

Table 1 Comparison of fluorescent probes for Hg²⁺

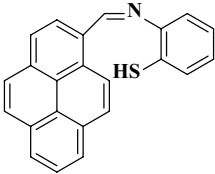
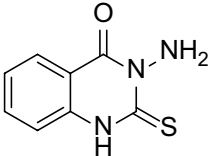
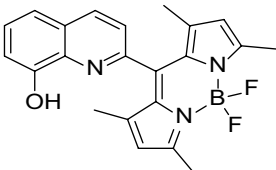
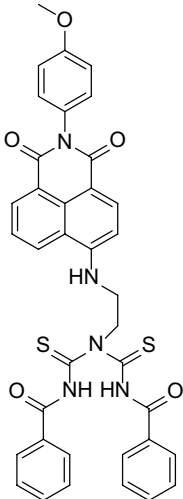
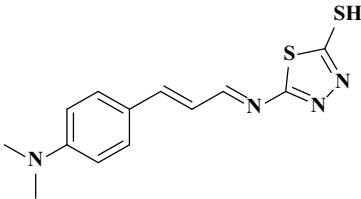
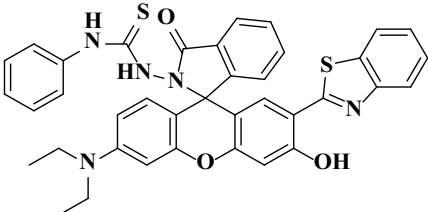
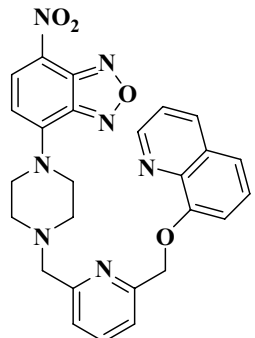
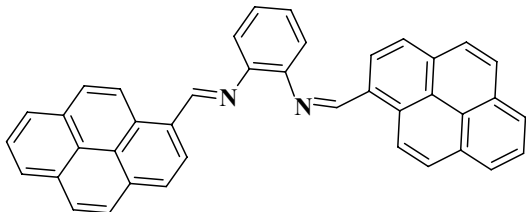
Sl. No	Sensor	Detection Limit (M)	Binding Constant (M ⁻¹)	Application	Reference
01		2.82×10^{-6}	7.36×10^4	Cell imaging	[33]
02		3.5×10^{-7}	4.54×10^2	Metal ion sensor and real sample analysis	[9]
03		5.0×10^{-6}	7.41×10^4	Metal ion sensor	[43]
04		0.83×10^{-6}	3.76×10^4	Cell imaging and water sample	[44]
05		2.0×10^{-6}	2.5×10^4	Water sample	[45]
06		0.27×10^{-6}	4.04×10^4	Cell imaging	[46]

Table 1 (continued)

Sl. No	Sensor	Detection Limit (M)	Binding Constant (M ⁻¹)	Application	Reference
07		1.92×10^{-8}	1.15×10^4	Cell imaging	[47]
		9.0×10^{-8}	1.29×10^5	Cell imaging and test strip application	Present work

132.16, 131.43, 130.83, 129.10, 127.85, 127.26, 126.50, 126.16, 125.44, 125.01, 124.84, 124.22, 123.30, 122.31, 111.98. IR (KBr, cm⁻¹) ν : 1587 (m. C=N), 3041 (Ar-H); ESI-MS: m/z 533.21 [(M+1)⁺].

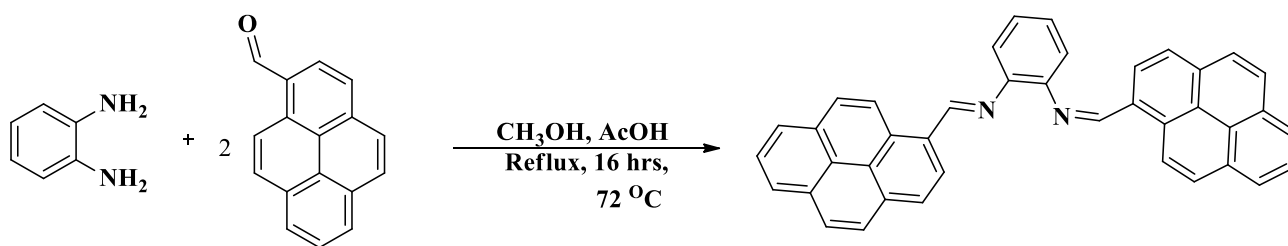
ν : 2969 (Ar-H), 1590 (br. C=N), 1513 (asym. OCO), 1236 (sym. OCO); ESI-MS: m/z 851.26 [(M+1)⁺].

Synthesis of Mercury(II) Complex (Scheme 2)

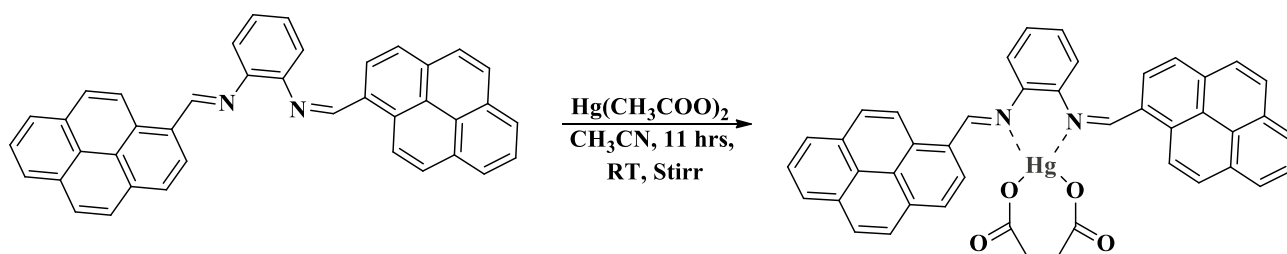
The synthesis of the mercury complex is induced by the dropwise addition of mercuric acetate (0.15 g, 0.41 mmol, in 10 mL MeCN) to the solution of PAMP (0.2 g, 0.37 mmol, in 15 mL MeCN) at room temperature with constant stirring. Upon addition of all the mercuric acetate, the reaction mixture turns to colorless and stirring was continued for further 11 h to get dark red solid. It was filtered, washed with MeOH and chloroform to get pure compound and dried in air. Yield: 0.18 g, 56%. Elem. Anal. Calculated for C₄₄H₃₀N₂O₄Hg²⁺: C, 62.14; H, 3.33; N, 3.56. Found: C, 62.11; H, 3.29; N, 3.52. IR (KBr, cm⁻¹)

General Procedure for UV-Visible and Fluorescence Experiments

The stock solutions of sensor (1.0×10^{-5} M) and metal nitrate solutions (1.0×10^{-3} M) were prepared in aqueous acetonitrile (2:8). The UV-Visible and fluorescence response of fifteen metal ions (Cd²⁺, Co²⁺, Hg²⁺, Cu²⁺, Mg²⁺, Mn²⁺, Ni²⁺, K⁺, Na⁺, Zn²⁺, Sr²⁺, Pb²⁺, Al³⁺, Cr³⁺ and Fe³⁺) was investigated. Selectivity of the probe has been tested for all the metal ions using both UV-Visible and fluorescence experiments. To a 2 mL of sensor, 10 equivalents of each metal ion solutions were introduced and stirred for 1 min before carrying out absorption and fluorescence measurements. The fluorescence and UV-Visible titrations were achieved by using varied concentrations (0–2 eq.) of metal



Scheme 1 Synthetic route of PAMP (L)



Scheme 2 Synthetic route for synthesis of Mercury(II) Complex

ion solution by maintaining the ligand concentration constant. The quantum yield (ϕ) of the sensor in presence and absence of the mercury(II) ions has been calculated according to the formula [48].

Preparation of Solutions for $^1\text{H-NMR}$ Titration

Stock solutions of ligand and mercuric nitrate were prepared in DMSO-d_6 for $^1\text{H-NMR}$ titrations.

Results and Discussion

UV–Visible and Fluorescence Spectral Studies of PAPM

The absorption and emission properties of the probe were measured using UV–Visible and fluorescence techniques in aqueous MeCN. At 275 and 355 nm, the probe showed two intense absorption bands, which can be assigned to pyrene based absorption bands. When the probe was excited at 355 nm, the pyrene based emission peaks (structured) were observed at 410 and 428 nm [41]. However, when the mercury(II) ions are added to the probe, a ratiometric shift was observed in the emission peak (non structured) at 456 nm with decrease in the fluorescence intensity. Furthermore, no significant changes in the emission peaks were noticed of probe after other metal ions were added to the sensor. The findings of fluorescence spectral studies of

probe with various metal ions reveal that the receptor only responds to Hg^{2+} (Fig. 1).

Fluorescence Titration Studies

The stock solutions of receptor and mercury(II) ions were prepared in same concentration which is used for UV–Visible measurements. Among all the tested metal ions, the probe showed extreme sensitivity to Hg^{2+} (Fig. 2). Fluorescence titration has been carried out for thorough understanding of binding properties of sensor towards Hg^{2+} . The probe exhibited substantially stronger fluorescence property ($\phi=0.236$) when irradiated at 365 nm. UV light, which can be perceived through naked eye. When mercury(II) ions were added to the probe solution, the ratiometric shift of emission band occurs at 456 nm with fluorescence quenching ($\phi=0.024$). Hence, PAPM functions as a potent “turn-off” sensor for determining mercury(II) ions. The quenching property of the probe has successively enhanced as the concentration of mercuric ions is increased in sequential order from 0–2 equivalent (0–40 μL) (Fig. 3).

Stoichiometry and Sensing Mechanism of PAPM with Hg^{2+}

ESI–MS spectrometry, Job’s plot experimental data, IR spectral studies and $^1\text{H-NMR}$ titration analysis confirm the formation of a complex between PAM and mercury(II)

Fig. 1 Fluorescence intensity of PAM with different metal ions (10 eq.) under irradiation at 365 nm. UV light



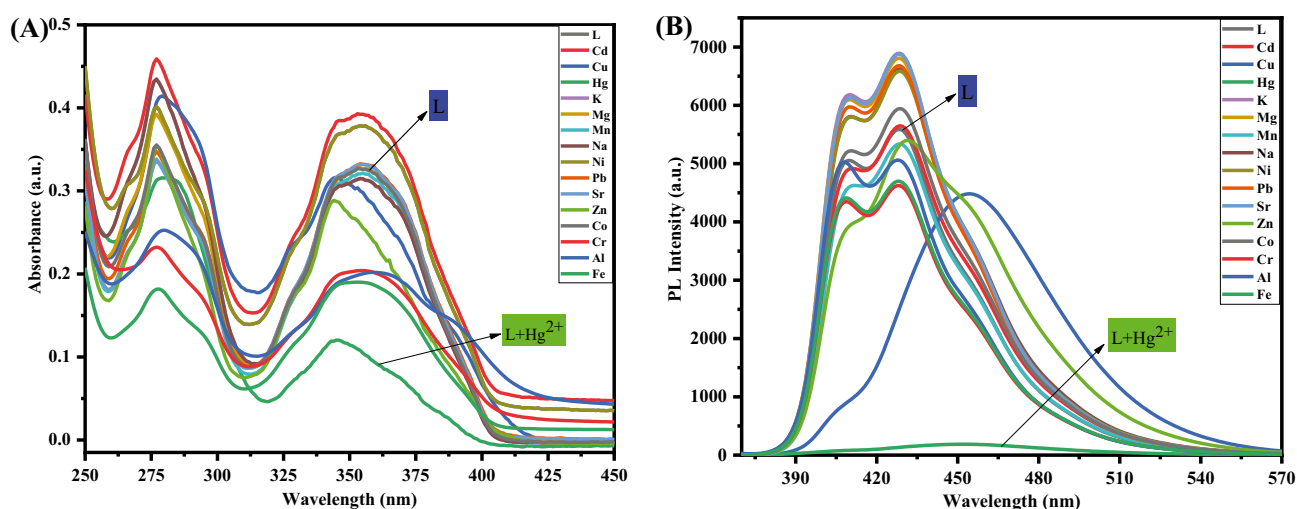


Fig. 2 **A** absorption and **B** fluorescence spectral changes of PAM (1.0×10^{-5} M) in the presence of 10 equivalent of diverse metal nitrates (1.0×10^{-3} M) in aqueous acetonitrile respectively

ion in a 1:1 ratio. The fluorescence quenching of probe towards Hg^{2+} results from chelation enhanced quenching (CHEQ) which can be attributed to significant spin–orbit coupling constant of the heavy mercury(II) ion [49]. Additionally, the ligand structure lacks intramolecular hydrogen bonding and the presence of nitrogen donor sites aids in direct interaction with the mercury(II) ion as depicted in Scheme 2. The presence of rigid electron rich pyrene groups boosts the chelating ability of the probe through two nitrogen lone pairs resulting in fluorescence quenching [49].

¹H-NMR titration studies were carried out in DMSO-*d*₆ to assess the change in the chemical shift of imine protons of ligand upon binding to Hg^{2+} . It is known fact that due to the electron donating nature of pyrene groups, the electron cloud is pulled towards both nitrogen atoms present in the fluorophore. The imine protons in the free ligand resonate at 9.50 ppm, after adding the 0.5 and 1 equivalent of mercury(II) ions to the free ligand, this peak shifted to 9.46 and 9.35 ppm respectively. This shift indicates the coordination of both nitrogen atoms to Hg^{2+} lead to decrease in electron density on nitrogen atoms [50] which is clearly indicated by upfield shift of imine protons by

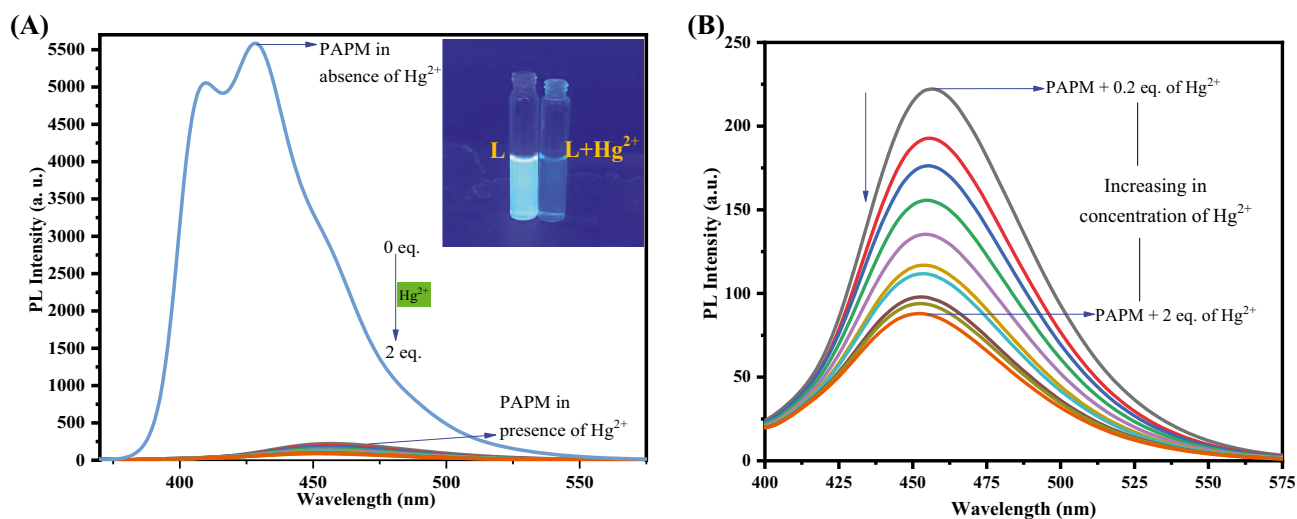
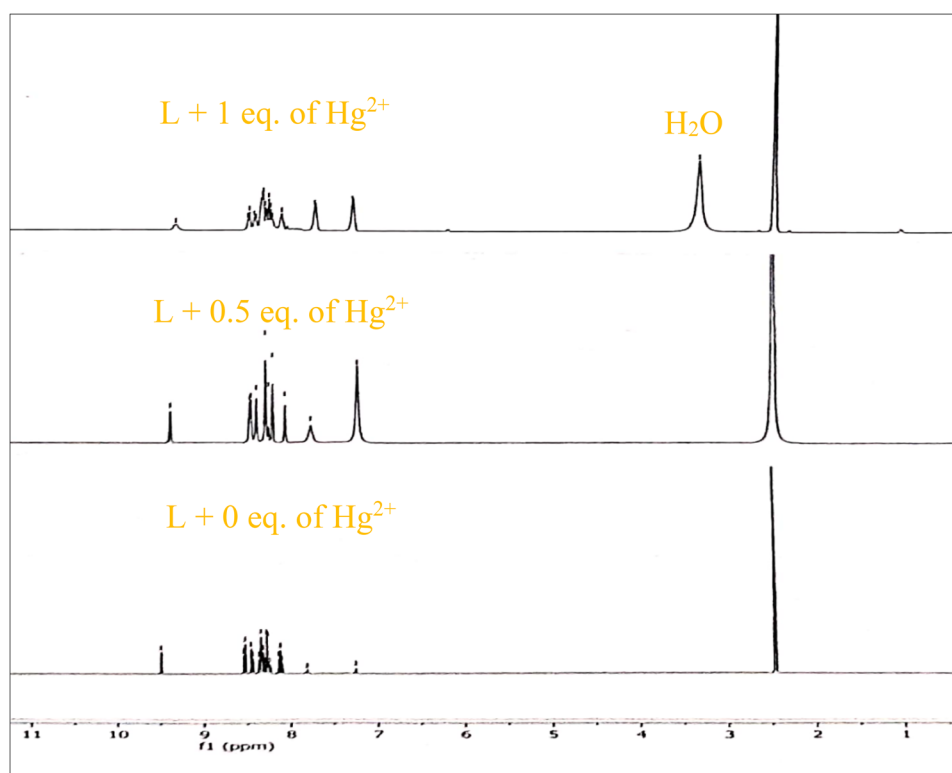


Fig. 3 **A** Fluorescence titration spectra of PAM (1.0×10^{-5} M) with increase in concentration of Hg^{2+} with an excitation at 355 nm in aqueous acetonitrile. Inset: Change in the color of luminescence and quenching in photoluminescence intensity (under 365 nm. UV lamp)

of probe after addition of mercury(II) ions (0–2 eq.) to PAM. **B** Expansion graph of fluorescence titration of PAM with increase in concentration of Hg^{2+}

Fig. 4 $^1\text{H-NMR}$ titration of PAPM with Hg^{2+}



0.15 ppm (Fig. 4). After addition of 1 eq. Hg^{2+} to the free ligand there is no appreciable change in chemical shifts of other protons.

The appearance of a peak with maximum intensity at 851.26 m/z in the ESI-MS (Fig. S4) further supports to 1:1 complex formation between the probe and the mercury(II) ions.

The IR spectrum was recorded to ensure the complex formation between PAPM and Hg^{2+} and also to confirm the binding mode of acetate ion. PAPM showed a band of medium intensity at 1587 cm^{-1} ($\text{C}=\text{N}$) and 3041 cm^{-1} (Ar-H) which have been shifted to 1590 and 2969 cm^{-1} respectively upon complexation with Hg^{2+} . The shift in the $\text{C}=\text{N}$ stretching frequency clearly suggests the coordination of nitrogen atoms with mercuric ion. The presence of two new bands at 1513 and 1236 cm^{-1} in the complex are assigned to asymmetric and symmetric stretching (νOCO) vibrations of acetate ions respectively and the difference of 276 cm^{-1} among these two bands suggests the unidentate coordination mode of acetate [51].

The Job's plot experiment [52] was carried out using stock solutions of PAPM and Hg^{2+} ($1.0 \times 10^{-4}\text{ M}$ in aqueous acetonitrile) to determine the affinity of mercury(II) ion towards PAPM. Using the plot of photoluminescence intensity v/s mole fraction (X_M) of the mercury(II) ions at 428 nm. (Fig. 5), the stoichiometry of PAPM and Hg^{2+} was established. The intersection point at $0.5 X_M$ in the

Job's plot clearly reveals 1:1 stoichiometry between PAPM and Hg^{2+} .

Limit of Detection (LOD) and Association Constant (K_a)

The value of the LOD was determined using standard deviation (SD) and slope obtained by linear fittings based on

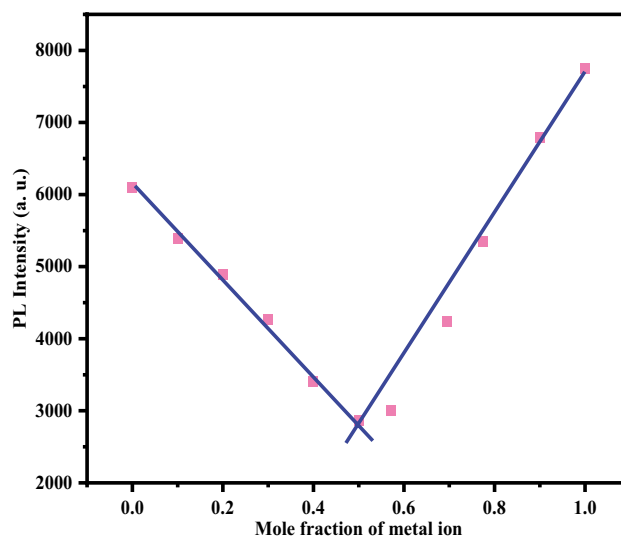


Fig. 5 Job's plot showing 1:1 stoichiometry between PAPM and Hg^{2+} . The molar ratio $[\text{Hg}^{2+}]/\{[\text{L}]+[\text{Hg}^{2+}]\}$ was displayed as a function of fluorescence intensity at 428 nm

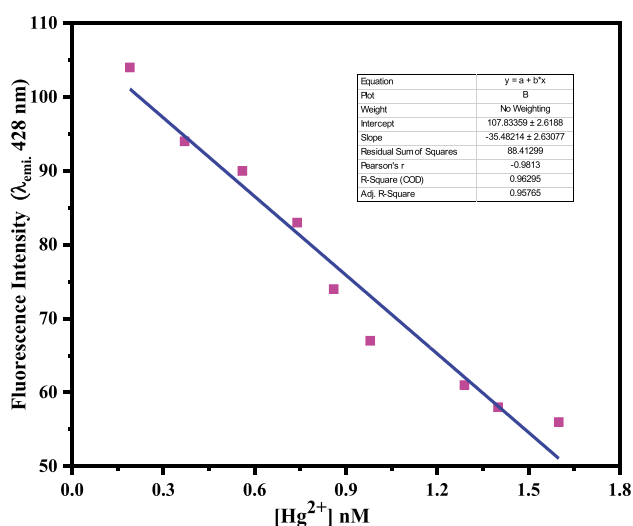
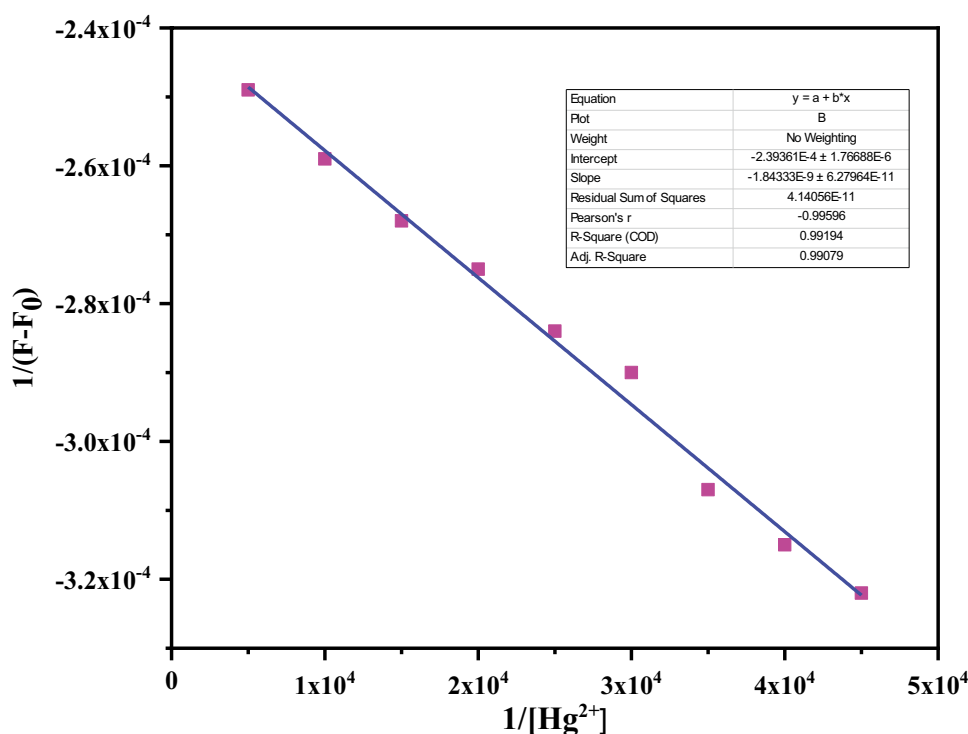


Fig. 6 Limit of detection based on fluorescence titration of PAPM with change in concentrations of Hg^{2+}

fluorescence titration studies by using $3\sigma/\text{slope}$ [53] (where σ refers to standard deviation of probe). The emission data at 428 nm was used to plot the graph of LOD (Fig. 6). The graph of relative fluorescence intensity versus concentration of mercury(II) ion suggests the detection limit of PAPM for Hg^{2+} as 9.0×10^{-8} M. The obtained LOD value is comparable to other reported methods [27–30].

The stability constant K_a was graphically evaluated using the Benesi-Hildebrand equation [54] by plotting

Fig. 7 Benesi-Hildebrand curve for PAPM with Hg^{2+}



$(1/F-F_0)$ versus $1/[\text{Hg}^{2+}]$ (Fig. 7), where F_0 denotes the fluorescence intensity of bare sensor and F denotes the maximum photoluminescent intensity as a function of Hg^{2+} concentration at 428 nm. The slope yielded the K_a value of $1.29 \times 10^5 \text{ M}^{-1}$ for PAPM towards Hg^{2+} .

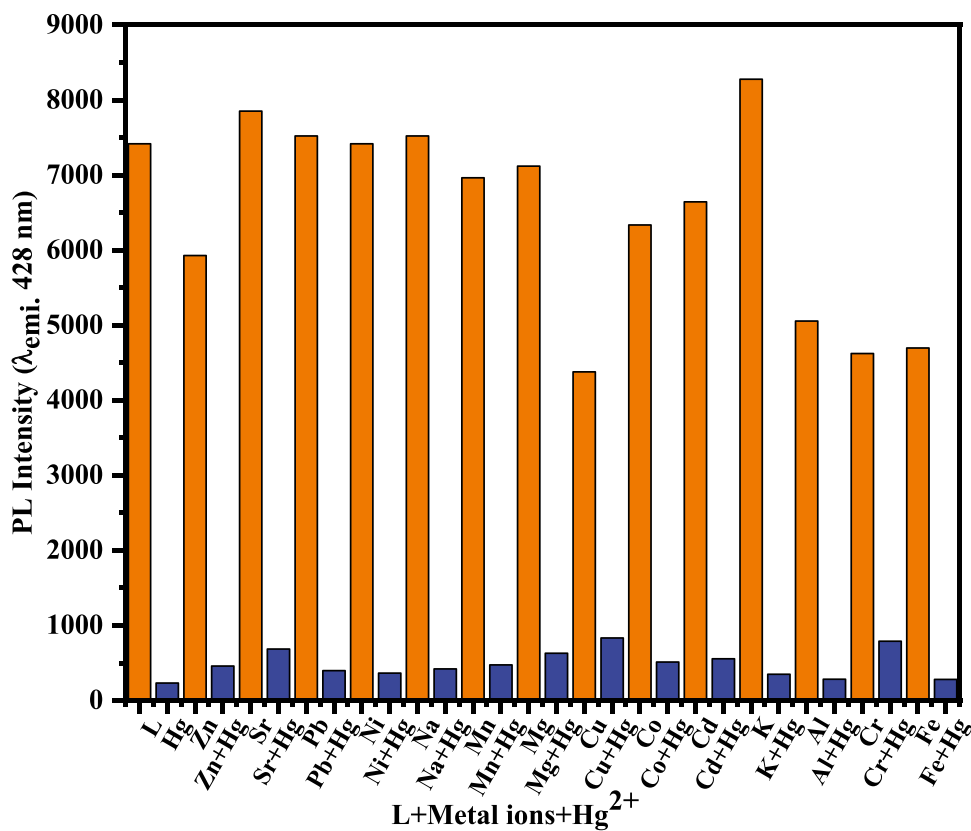
Competitive Study of Counter Metal Ions

To demonstrate the high selectivity of PAPM and to assess its practical application towards Hg^{2+} , we also performed competitive studies in the presence of other fifteen metal ions (10 equivalent) at concentration of $10 \mu\text{M}$ Hg^{2+} (Fig. 8). These tests reveal that none of the specified ions significantly obstruct the detection of Hg^{2+} by PAPM.

pH Studies

The fluorescence response of receptor towards Hg^{2+} was investigated at various pH levels as the effect of pH is vital for practical aspects of sensing. Buffer solutions ranging from 3.0 to 11.0 were prepared to test the pH sensitivity of the sensor (1.0×10^{-5} M) for the determination of mercury(II) ion (1.0×10^{-3} M) using phosphate buffer saline (PBS) environment. The mercury(II) ion was introduced to the buffered PAPM solution and the results showed that PAPM can effectively bind to Hg^{2+} in the

Fig. 8 Bar graph showing the relative photoluminescence intensity of PAMP (1.0×10^{-5} M) with Hg^{2+} in presence of 10 equivalent of other interfering metal ions (1.0×10^{-3} M) in $\text{MeCN}:\text{H}_2\text{O}$ (8:2)



pH range of 3.0–11.0 with no discernible changes in the fluorescence spectra (Fig. 9).

Cytotoxicity by MTT Assay

HeLa cells purchased from National Center for Cell Science, Pune, India. The cells were seeded in a 96-well flat-bottom microplate and maintained at 37 °C in 95% humidity and 5% CO_2 overnight. Different concentration (100, 50, 25, 12.5, 6.25 and 3.125 $\mu\text{g}/\text{ml}$) of PAMP in presence and absence of Hg^{2+} were treated. The cells were incubated further for 8 h. The wells were washed twice with PBS and 20 μL of the MTT staining solution was added to each well and plate was incubated at 37 °C. After 4 h, 100 μL of DMSO was added to each well to dissolve the formazan crystals and absorbance was recorded with a 570 nm using microplate reader. As a result of the MTT analysis, it was found that the PAMP was cytotoxic at higher concentrations but less toxic at lower concentrations. Cell viability was greater than 98% at a lower concentration of PAMP (3.125 μM), while it was 42.43% control at a higher concentration (100 μM). Despite of this, over 80% of the cells were continued to survive after PAMP concentration was increased to 12.5 μM . (Fig. S9).

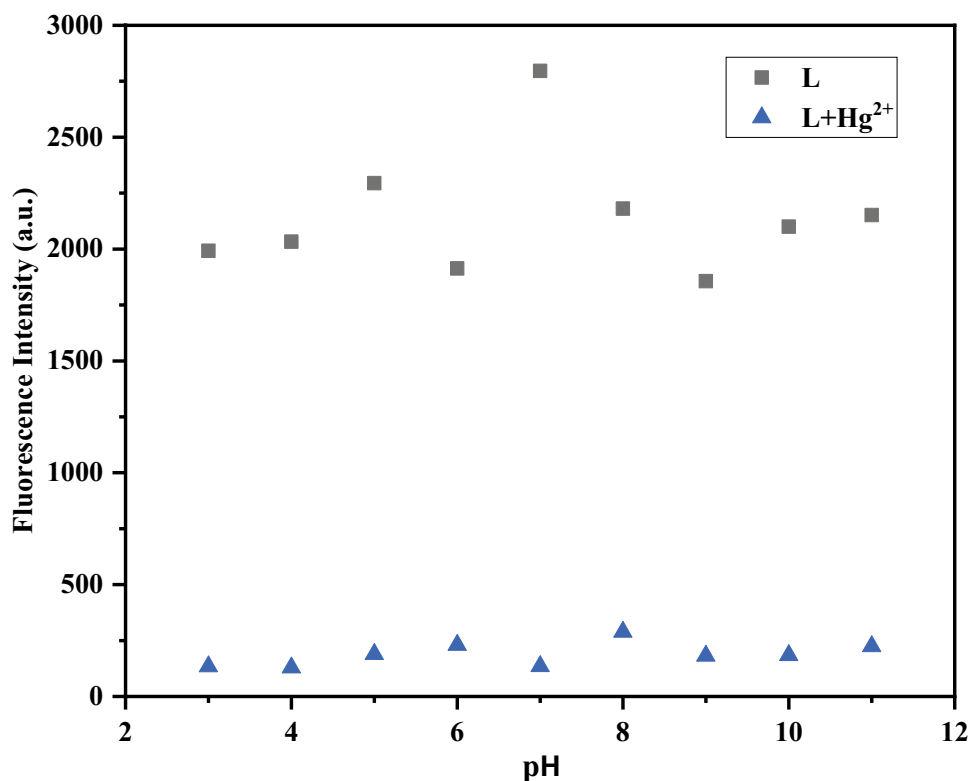
Cell Imaging Studies

HeLa cells were sown separately on 16 mm coverslips and allowed to grow for 24 h in order to conduct bio-imaging experiment. Separate incubations of 10 μM of each compound were placed for 60 min at 37 °C in the dark. After removing the medium, the cells underwent three PBS washes before being fixed for 30 min with 4% para-formaldehyde. After that, a Zeiss LSM 710 confocal microscope was used to record the fluorescence of the cells. According to fluorescence imaging experimental results, PAMP exhibits high fluorescence, but when Hg^{2+} are added, the fluorescence intensity is quenched due to the combination of PAMP with Hg^{2+} in live HeLa cells (Fig. 10).

Sensing with Test Strips and TLC Plates

In order to explore the sensing properties of the probe towards mercury(II) ions in aqueous acetonitrile, we conducted the experiments on test strips as well as silica gel coated TLC plates for the practical utility. The four test strips (A to D; Fig. 11) were prepared by dipping test strips in PAMP solution (A), in PAMP and Hg^{2+} solution (B), in

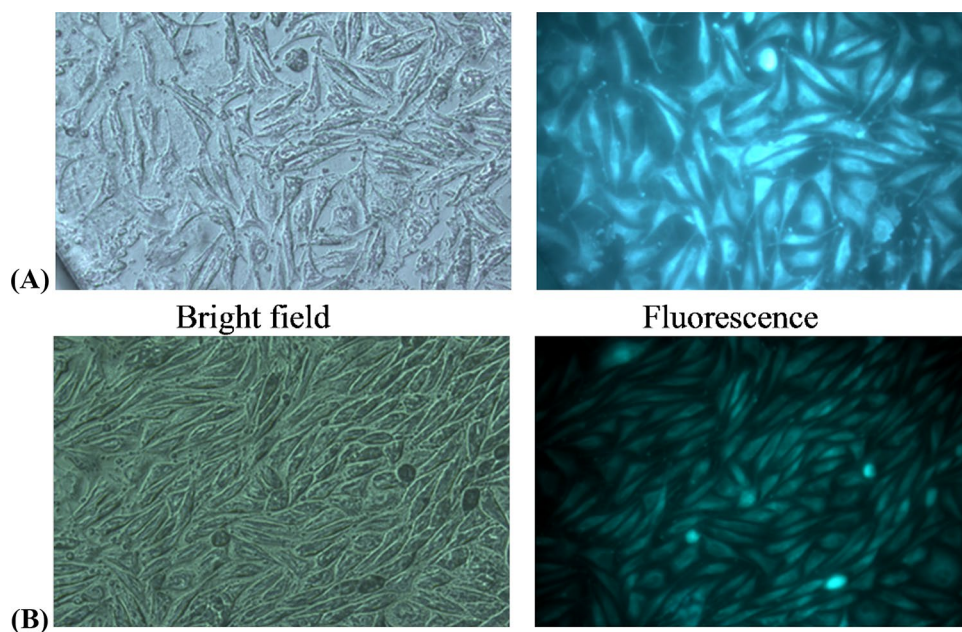
Fig. 9 Fluorescence response of receptor to Hg^{2+} (10 eq.) with different ranges of pH (3.0–11.0) solutions of phosphate buffer saline



PAPM and various metal ion solution (C) and in solutions of PAPM, various metal ion and Hg^{2+} ion (D). Later these test strips were kept to dry at room temperature and exposed to UV lamp. This experimental results clearly illustrate that the color of the test strip changes from intense white luminescence (in the absence of Hg^{2+}) to pale blue green color (minimum/almost no fluorescence) after irradiation at 365 nm.

The sensing application of receptor was also performed using a couple of TLC plates by immersing one of them in PAPM solution and other in the solutions of PAPM and mercury(II) ions sequentially. Further, both TLC plates were allowed to dry at room temperature for 20 min before being exposed to UV radiations at 365 nm. The TLC plate dipped in PAPM solution exhibited deep bluish white fluorescence

Fig. 10 Fluorescence image of HeLa cells **A** incubated with PAPM (10 μM) for 1 h, **B** incubated with PAPM for 1 h and then Hg^{2+} (5 μM) for 1 h



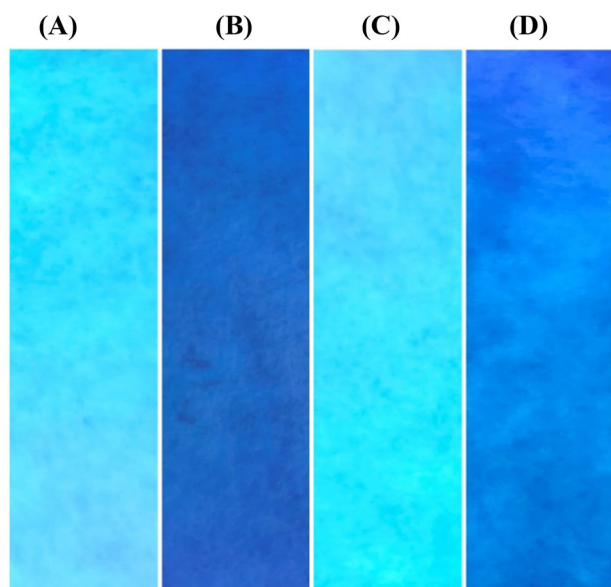


Fig. 11 **A** Test strip image after immersed in PAMP (high fluorescent). **B** Test strip image of (A) after immersed in 10 eq. of aqueous acetonitrile solution of Hg^{2+} (non-fluorescent). **C** Test strip image after immersed in PAMP in presence of other metal ions used in selectivity experiment (high fluorescent). **D** Test strip image of (C) after dipped in aqueous acetonitrile solution of Hg^{2+} (non-fluorescent). All test strips photographs were captured under irradiation at 365 nm

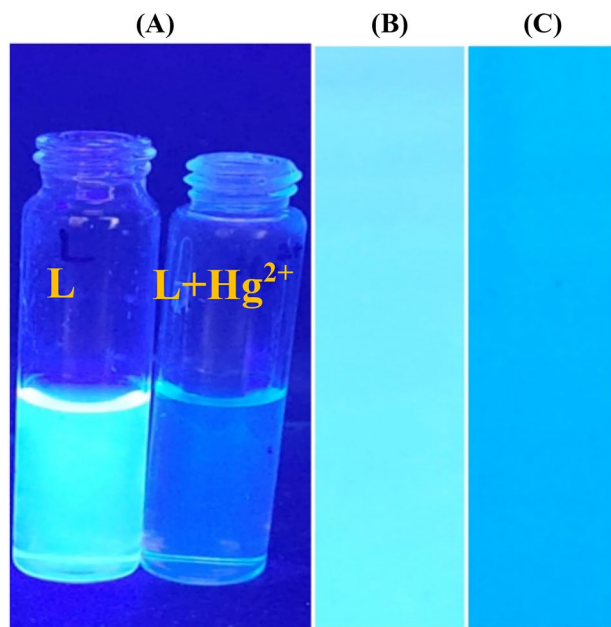


Fig. 12 **A** Change in fluorescence intensity and its color. **B** Image of TLC plate dipped in PAMP solution showing intense fluorescence. **C** Image of TLC plate immersed in PAMP solution followed by immersion in Hg^{2+} solution diminishing the fluorescence. (All images were captured under irradiation at 365 nm and solutions were prepared in aqueous MeCN)

(Fig. 12B), while another TLC plate displayed pale blue-green which is non-fluorescent in nature (Fig. 12C) (Fig. 12).

The successful usage of less expensive test strip and TLC plate techniques illustrates potential of the probe to recognize mercury(II) ions in future aspects.

Conclusion

The present study illustrates the synthesis of novel (N^1E,N^2E)- N^1,N^2 -bis(pyrene-1-ylmethylene)benzene-1,2-diamine (PAMP) as a sensor to detect Hg^{2+} fluorometrically in aqueous MeCN. In presence of Hg^{2+} , receptor experiences quenching in fluorescence intensity as well as a ratiometric redshift in the emission spectrum. The LOD and association constant (K_a) of sensor for Hg^{2+} were found to be 9.0×10^{-8} M and $1.29 \times 10^5 \text{ M}^{-1}$ respectively. The novel probe can be used for live cell imaging studies for detection of mercury(II) ions in HeLa cells. The present report also explored the sensing applications using low cost test strips and TLC plates for the detection of noxious mercuric ions. In summary, we conclude that the probe could serve as a potential sensor for the detection of mercury(II) ions.

Abbreviations DMSO: Dimethylsulphoxide; WBGs: Wide-band gap semiconductors; eV: Electron Volt; τ : Decay time; I_0 and I : Luminescence intensities at time 0 and t ; MHz: Megahertz; $^\circ\text{C}$: Degree Celsius; $^\circ\text{C}/\text{min}$: Degree Celsius per minute; mmol: Millimol; mL: Milliliter; $F(R_\infty)$: Kubelka–Munk function; C: Constant of proportionality; %: Percentage; S: Scattering coefficient; K: Absorption coefficient; N: Frequency; Δ : Chemical shift on delta scale; ΔE_0 : Energy gap between excited singlet and triplet state; ΔE_1 : Energy gap between excited triplet state and resonating level; Nm: Nanometer; S_0 : Ground singlet; S_1 : Excited singlet state; T_1 : Excited triplet state; KBr: Potassium bromide; x and y: Color coordinates of sample; ppm: Parts per million; OLEDs: Organic light emitting diodes; $\mu\text{g}/\text{mL}$: Microgram per milliliter; PFA: 5-Phenyl 2-furoic acid; mmol/L: Millimol per liter; phen: 1,10-Phenanthroline; batho: Bathophenanthroline; bipy: 2,2-Bipyridyl; Sm^{3+} : Trivalent samarium ion; Gd: Gadolinium metal; DR: Diffuse reflectance; E_g : Band-gap energy; $^1\text{H-NMR}$: Proton nuclear magnetic resonance; h : Planck's constant; PL: Photoluminescence; FT-IR: Fourier transform infra-red; TG and DTG: Thermal and differential thermogravimetric; $^1\text{H-NMR}$: Proton nuclear magnetic resonance; UV-vis: Ultraviolet-visible; CIE: Commission International de l'Eclairage

Supplementary Information The online version contains supplementary material available at <https://doi.org/10.1007/s10895-022-03066-2>.

Acknowledgements The author KBG is thankful to UGC, New Delhi for providing Mid-Career Award Grant [F.19-268/2021 (BSR)] and Chethanakumar is grateful to Karnatak University, Dharwad for awarding University Research Studentship and thankful to USIC, K.U. Dharwad for facilitating instrumentation facility.

Author's Contributions Chethanakumar: Molecule designing, analysis of spectroscopic data, application study, writing original manuscript. Mahantesh Budri: Formal analysis. Kalagouda B. Gudasi: Supervision, corresponding author, formal correction. Ramesh S.

Vadavi: Editing, validation of the manuscript. **Satish S. Bhat:** Revising the manuscript.

Funding University Grants Commission of India, Mid-Career Award Grant [F.19–268/2021 (BSR)].

Data Availability Not applicable.

Declarations

Ethical Approval Not applicable.

Competing Interests There are no conflicts of interest to declare.

Conflicts of Interest There are no conflicts of interest to declare.

References

- Kumar A, Dubey M, Pandey R, Gupta RK, Kumar A, Kalita ACh, Pandey DS (2014) A schiff base and its copper(II) complex as a highly selective chemodosimeter for mercury(II) involving preferential hydrolysis of aldimine over an ester group. *Inorg Chem* 53:4944–4955. <https://doi.org/10.1021/ic403149b>
- Ma L-J, Liu J, Deng L, Zhao M, Deng Z, Li X, Tang J, Yang L (2014) Selective and sensitive fluorescence-shift probes based on two dansyl groups for mercury(II) ion detection. *Photochem Photobiol Sci* 13:1521–1528. <https://doi.org/10.1039/C4PP00094C>
- Hu JH, Li JB, Qi J, Chen JJ (2015) Highly selective and effective mercury(II) fluorescent sensors. *New J Chem* 39:843–848. <https://doi.org/10.1039/C4NJ01147C>
- Boening DW (2000) Ecological effects, transport, and fate of mercury: a general review. *Chemosphere* 40:1335–1351. [https://doi.org/10.1016/S0045-6535\(99\)00283-0](https://doi.org/10.1016/S0045-6535(99)00283-0)
- Wanga Q, Kima D, Dionysioua DD, Soriala GA, Timberlake D (2004) Sources and remediation for mercury contamination in aquatic systems—a literature review. *Environ Pollut* 131:323–336. <https://doi.org/10.1016/j.envpol.2004.01.010>
- Clarkson TW, Magos L, Myers GJ (2003) The toxicology of mercury—current exposures and clinical manifestations. *N Engl J Med* 349:1731–1737. <https://doi.org/10.1056/NEJMr022471>
- Fitzgerald WF, Lamborg CH, Hammerschmidt CR (2007) Marine biogeochemical cycling of mercury. *Chem Rev* 107:641–662. <https://doi.org/10.1021/cr050353m>
- Song F, Yang C, Shao X, Lei Du, Zhu J, Kan C (2019) A reversible “turn-off-on” fluorescent probe for real-time visualization of mercury(II) in environmental samples and its biological applications. *Dyes Pigm* 165:444–450. <https://doi.org/10.1016/j.dyepig.2019.02.054>
- Anand T, Sivaraman G, Chellappa D (2014) Hg₂⁺ mediated quinazoline ensemble for highly selective recognition of Cysteine. *Spectrochim Acta Part A Mol Biomol Spectrosc* 123:18–24. <https://doi.org/10.1016/j.saa.2013.12.054>
- Huang W, Zhang S (2002) Determination of mercury at a dithizone-modified glassy carbon electrode by anodic stripping voltammetry. *Anal Sci* 18:187–189. <https://doi.org/10.2116/analsci.18.187>
- Nam D-H, Basu N (2011) Rapid methods to detect organic mercury and total selenium in biological samples. *Chem Cent J* 5. <https://doi.org/10.1186/1752-153X-5-3>
- Clevenger WL, Smith BW, Winefordner JD (1997) Trace determination of mercury: a review. *Crit Rev Anal Chem* 27:1–26. <https://doi.org/10.1080/10408349708050578>
- Suvarapu LN, Seo Y-K, Baek S-O (2013) Speciation and determination of mercury by various analytical techniques. *Rev Anal Chem* 32:225–245. <https://doi.org/10.1515/revac-2013-0003>
- Aydin D (2018) A turn OFF fluorescent probe for selective detection of Hg₂⁺ ions. *Eur J Sci Technol* 17:483–490. <https://doi.org/10.31590/ejosat.634119>
- Rama Devi P, Gangaiah T, Naidu GRK (1991) Determination of trace metals in water by neutron activation analysis after preconcentration on a poly(acrylamidoxime) resin. *Anal Chem Acta* 249:533–537. [https://doi.org/10.1016/S0003-2670\(00\)83030-5](https://doi.org/10.1016/S0003-2670(00)83030-5)
- Pandey R, Gupta RK, Shahid M, Maiti B, Misra A, Pandey DS (2012) Synthesis and characterization of electroactive ferrocene derivatives: ferrocenylimidazoquinazoline as a multichannel chemosensor selectively for Hg₂⁺ and Pb₂⁺ ions in an aqueous environment. *Inorg Chem* 51:298–311. <https://doi.org/10.1021/ic201663m>
- Varnes AW, Barry Dodson R, Wehry EL (1972) Interactions of transition-metal ions with photoexcited states of flavins. Fluorescence quenching studies. *J Am Chem Soc* 94:946–950. <https://doi.org/10.1021/ja00758a037>
- Prodi L, Bargossi C, Montalti M, Zaccheroni N, Ning Su, Bradshaw JS, Izatt RM, Savage PB (2000) An effective fluorescent chemosensor for mercury ions. *J Am Chem Soc* 122:6769–6770. <https://doi.org/10.1021/ja0006292>
- Nolan EM, Racine ME, Lippard SJ (2006) Selective Hg(II) detection in aqueous solution with thiol derivatized fluoresceins. *Inorg Chem* 45:2742–2749. <https://doi.org/10.1021/ic052083w>
- Coskun A, Akkaya EU (2006) Signal ratio amplification via modulation of resonance energy transfer: proof of principle in an emission ratiometric Hg(II) sensor. *J Am Chem Soc* 128:14474–14475. <https://doi.org/10.1021/ja066144g>
- Guo X, Qian X, Jia L (2004) A highly selective and sensitive fluorescent chemosensor for Hg₂⁺ in neutral buffer aqueous solution. *J Am Chem Soc* 126:2272–2273. <https://doi.org/10.1021/ja037604y>
- Ho M-L, Chen K-Y, Lai-Chin Wu, Shen J-Y, Lee G-H, Ko M-J, Wang C-C, Lee J-F, Chou P-T (2008) Diaza-18-crown-6 appended dual 7-hydroxyquinolines; mercury ion recognition in aqueous solution. *Chem Commun* 21:2438–2440. <https://doi.org/10.1039/B801366G>
- Goshisht MK, Patra GK, Tripathi N (2022) Fluorescent Schiff base sensors as a versatile tool for metal ion detection: strategies, mechanistic insights, and applications. *Mater Adv* 3:2612–2669. <https://doi.org/10.1039/D1MA01175H>
- Khan S, Chen X, Almahri A, Allehyani ES, Alhumaydhi FA, Ibrahim MM, Ali S (2021) Recent developments in fluorescent and colorimetric chemosensors based on schiff bases for metallic cations detection: a review. *J Environ Chem Eng* 9:106381. <https://doi.org/10.1016/j.jece.2021.106381>
- Shellaiah M, Chen Y-T, Thirumalaivasan N, Aazaad B, Awasthi K, Sun KW, Shu-Pao Wu, Lin M-C, Ohta N (2021) Pyrene-based AIEE active nanoprobe for Zn₂⁺ and tyrosine detection demonstrated by DFT, bioimaging, and organic thin-film transistor. *ACS Appl Mater Interfaces* 13:28610–28626. <https://doi.org/10.1021/acsami.1c04744>
- Jali BR, Baruah JB (2021) Recent progress in Schiff bases in detections of fluoride ions. *Dyes Pigm* 194:109575. <https://doi.org/10.1016/j.dyepig.2021.109575>
- Shiraishi Y, Sumiya S, Hirai T (2010) A coumarin–thiourea conjugate as a fluorescent probe for Hg(II) in aqueous media with a broad pH range 2–12. *Org Biomol Chem* 8:1310–1314. <https://doi.org/10.1039/B924015B>
- Wang H-F, Shu-Pao Wu (2013) Highly selective fluorescent sensors for mercury(II) ions and their applications in living cell imaging. *Tetrahedron* 69:1965–1969. <https://doi.org/10.1016/j.tet.2012.12.075>

29. Ge J-Z, Zou Y, Yan Y-H, Lin S, Zhao X-F, Cao Q-Y (2016) A new ferrocene–anthracene dyad for dual-signaling sensing of Cu(II) and Hg(II). *J Photochem Photobiol A: Chem* 315(2016):67–75. <https://doi.org/10.1016/j.jphotochem.2015.09.011>
30. Muthukumar V, Kulathulyer S (2020) Twisted pyrene with perfect hetero atomic cavity optical sensor for Hg₂²⁺ and Pb²⁺. *Inorg Chem Commun* 121:108187. <https://doi.org/10.1016/j.inoche.2020.108187>
31. Erguna EGC, Ertas G, Eroglu D (2020) A benzimidazole-based turn-off fluorescent sensor for selective detection of mercury (II). *J Photochem Photobiol A: Chem* 394:112469. <https://doi.org/10.1016/j.jphotochem.2020.112469>
32. Shellaiah M, Rajan YC, Balu P, Murugan A (2015) A pyrene based Schiff base probe for selective fluorescence turn-on detection of Hg₂⁺ ions with live cell application. *New J Chem* 39:2523–2531. <https://doi.org/10.1039/C4NJ02367F>
33. Ni X-L, Yanan Wu, Redshaw C, Yamato T (2014) Direct evidence of a blocking heavy atom effect on the water-assisted fluorescence enhancement detection of Hg₂⁺ based on a ratiometric chemosensor. *Dalton Trans* 43:12633–12638. <https://doi.org/10.1039/C4DT01310G>
34. Ewntie AM (2019) A review on fluorescent chemosensors for mercury (II) ion: mechanism and applications. *Int J Eng Sci Comput* 9:24182–24190
35. Martinez R, Espinosa A, Tarraga A, Molina P (2005) New Hg₂⁺ and Cu₂⁺ selective chromoand fluoroionophore based on a bichromophoric azine. *Org Lett* 7:5869–5872. <https://doi.org/10.1021/ol052508i>
36. Wua Y-S, Li C-Y, Li Y-F, Li D, Li Z (2016) Development of a simple pyrene-based ratiometric fluorescent chemosensor for copper ion in living cells. *Sensors Actuators B* 222:1226–1232. <https://doi.org/10.1016/j.snb.2015.06.151>
37. Lianga J, Liua H-B, Wang J (2019) Pyrene-based ratiometric and fluorescent sensor for selective Al³⁺ detection. *Inorg Chim Acta* 489:61–66. <https://doi.org/10.1016/j.ica.2019.02.009>
38. Sivaraman G, Anand T, Chellappa D (2012) Development of a pyrene based “turn on” fluorescent chemosensor for Hg₂⁺. *RSC Adv* 2:10605–10609. <https://doi.org/10.1039/C2RA21202A>
39. Dalbera S, Kulovi S, Dalai S (2018) Pyrene-based schiff base as selective chemosensor for copper(II) and sulfide ions. *ChemistrySelect* 3:6561–6569. <https://doi.org/10.1002/slct.201801205>
40. Shellaiah M, Yen-Hsing Wu, Singh A, RamakrishnamRaju MV, Lin H-C (2013) Novel pyrene- and anthracene-based Schiff base derivatives as Cu₂⁺ and Fe³⁺ fluorescence turn-on sensors and for aggregation induced emissions. *J Mater Chem A* 1:1310–1318. <https://doi.org/10.1039/C2TA00574C>
41. Jiang W, Wang W (2009) A selective and sensitive “turn-on” fluorescent chemodosimeter for Hg₂⁺ in aqueous media via Hg₂⁺ promoted facile desulfurization–lactonization reaction. *Chem Commun* 26:3913–3915. <https://doi.org/10.1039/B903606G>
42. Gao Y, Song J, Wang W (2011) A novel azobenzene-based fluorescent sensor for selective detection of mercury ion. *Lett Org Chem* 8:749–751. <https://doi.org/10.2174/157017811799304223>
43. Moon SY, Cha NR, Kim YH, Chang S-K (2004) New Hg₂⁺-selective chromo- and fluoroionophore based upon 8-hydroxyquinoline. *J Org Chem* 69:181–183. <https://doi.org/10.1021/jo034713m>
44. Ye F, Liang X-M, Ke-Xin Xu, Pang X-X, Chai Q, Ying Fu (2019) A novel dithiourea-appended naphthalimide “on-off” fluorescent probe for detecting Hg₂⁺ and Ag⁺ and its application in cell imaging. *Talanta* 200:494–502. <https://doi.org/10.1016/j.talanta.2019.03.076>
45. Singh R, Das G (2018) Fluorogenic detection of Hg₂⁺ and Ag⁺ ions via two mechanistically discrete signal genres: a paradigm of differentially responsive metal ion sensing. *Sensors Actuators B* 258:478–483. <https://doi.org/10.1016/j.snb.2017.11.097>
46. Chen S, Wang W, Yan M, Qin Tu, Chen S-W, Li T, Yuan M-S, Wang J (2018) 2-Hydroxy benzothiazole modified rhodol: aggregation-induced emission and dual-channel fluorescence sensing of Hg₂⁺ and Ag⁺ ions. *Sensors Actuators B* 255:2086–2094. <https://doi.org/10.1016/j.snb.2017.09.008>
47. Wang JH, Liu YM, Dong ZM, Chao JB, Hui Wang Yu, Wang SS (2020) New colorimetric and fluorometric chemosensor for selective Hg₂⁺ sensing in a near-perfect aqueous solution and bioimaging. *J Hazard Mater* 382:121056. <https://doi.org/10.1016/j.jhazmat.2019.121056>
48. Caspar JV, Meyer TJ (1983) Photochemistry of tris(2,2'-bipyridine) ruthenium(2+) ion (Ru(bpy)₃²⁺). Solvent effects. *J Am Chem Soc* 105:5583–5590. <https://doi.org/10.1021/ja00355a009>
49. Lee H, Lee H-S, Reibenspies JH, Hancock RD (2012) Mechanism of “turn-on” fluorescent sensors for mercury(II) in solution and its implications for ligand design. *Inorg Chem* 51:10904–10915. <https://doi.org/10.1021/ic301380w>
50. Zhou Y, Zhou H, Ma T, Zhang J, Niu J (2012) A new Schiff base based on vanillin and naphthalimide as a fluorescent probe for Ag⁺ in aqueous solution. *Spectrochim Acta Part A Mol Biomol Spectrosc* 88:56–59. <https://doi.org/10.1016/j.saa.2011.11.054>
51. Nakamoto K (2009) Infrared and raman spectra of inorganic and coordination compounds: Part A: theory and applications in inorganic chemistry, 6th edn. <https://doi.org/10.1002/9780470405840>
52. Tamil Selvan G, Varadaraju C, TamilSelvan R, Enoch IVMV, MosaeSelvakumar P (2018) On/off fluorescent chemosensor for selective detection of divalent iron and copper ions: molecular logic operation and protein binding. *ACS Omega* 3:7985–7992. <https://doi.org/10.1021/acsomega.8b00748>
53. Budri M, Kadolkar P, Gudasi K, Inamdar S (2019) A highly selective and sensitive turn on optical probe as a promising molecular platform for rapid detection of Zn (II) ion in acetonitrile medium: experimental and theoretical investigations. *J Mol Liq* 283:346–358. <https://doi.org/10.1016/j.molliq.2019.03.097>
54. Xie H-F, Yu C-J, Huang Y-L, Xu H, Zhang Q-L, Sun X-H, Feng X, Redshaw C (2020) A turn-off fluorescent probe for the detection of Cu₂⁺ based on a tetraphenylethylenefunctionalized salicylaldehyde Schiff-base. *Mater Chem Front* 4:1500–1506. <https://doi.org/10.1039/C9QM00759H>

Publisher's Note Springer Nature remains neutral with regard to jurisdictional claims in published maps and institutional affiliations.

Springer Nature or its licensor (e.g. a society or other partner) holds exclusive rights to this article under a publishing agreement with the author(s) or other rightsholder(s); author self-archiving of the accepted manuscript version of this article is solely governed by the terms of such publishing agreement and applicable law.